INT. J. HYPERTHERMIA, 1987, VOL. 3, NO. 3, 269–279

Determination of power deposition patterns for localized hyperthermia: a steady-state analysis

K. B. OCHELTREE and L. A. FRIZZELL

Bioacoustics Research Laboratory, University of Illinois, 1406 West Green Street, Urbana, Illinois 61801, U.S.A.

(*Received 13 August 1986; accepted 12 December 1986*)

Hyperthermia applicator design has concentrated on developing systems that allow control of power deposition patterns. In this paper, a method is detailed which uses the steady-state bioheat transfer equation and the target temperature distributions in normal and tumour tissue to calculate the desired steady-state power deposition patterns. This prospective thermal dosimetry approach is demonstrated analytically for three tumour models: an infinite half-space model; an infinite cylinder model; and a spherical model. A three-dimensional numerical method is demonstrated for two different tumour geometries and further applications of this method are discussed.

Key words: hyperthermia, uniform temperature, power deposition, bioheat transfer equation, steady state.

1. Introduction

Localized hyperthermic treatment of tumours has been accomplished with both invasive and non-invasive systems. Invasive techniques include the use of ferromagnetic seeds (Stauffer *et al.* 1984) and interstitial microwave antennas (Taylor 1980). Numerous non-invasive applicator systems have been employed which use several different modalities including magnetic induction (Storm *et al.* 1980, Oleson 1984), microwaves (Kantor 1981), and ultrasound (Christensen and Durney 1981, Hynynen 1986). More recent implementations of these techniques allow more precise control of the power deposition pattern. To fully employ the increased flexibility of these systems, it is desirable to determine the power deposition pattern required to treat a specific tumour most effectively.

The bioheat transfer equation has been successfully applied to the prediction of the temperature elevation produced by hyperthermia applicators in the presence of blood perfusion (Cravalho *et al.* 1980, Dickinson 1984, Roemer *et al.* 1984, Strohbehn and Roemer 1984) and its limitations have been discussed (Chen and Holmes 1980, Bowman 1981, Jain 1983). The following analysis will use the bioheat transfer equation to provide a first approximation to the effects of blood perfusion. In general, the time-dependent bioheat transfer equation must be used to determine the change in temperature with time. However, since much of a hyperthermia treatment period involves the maintenance of a steady temperature, the steady-state heating conditions are evaluated in this paper. For this, the bioheat transfer equation can be applied in its steady-state form:

$$0 = K\nabla^2 T - W_b C_b T + Q_p \tag{1}$$

where K is the thermal conductivity of the tissue (W/m/°C), T is the tissue temperature relative to the arterial blood temperature (°C), W_b is the blood perfusion rate (kg/m^3/s), C_b is the specific heat of blood (J/kg/°C), and Q_p is the local power deposition (W/m^3).

In the application of eqn (1) to comparative thermal dosimetry, a power deposition pattern is used to calculate the resultant temperature distribution. This approach works well for determining the temperature field produced by a given applicator or scan path, in the case of a scanned focal region produced by ultrasound or microwaves. However, such an approach yields no direct information regarding the placement of interstitial sources, best applicator design, or most appropriate scan path to achieve a desired temperature distribution in a given tumour.

From a clinical perspective, it is preferable to choose the desired temperature distribution and use a hyperthermia applicator to produce that distribution, as nearly as possible. The first step in the process is the calculation of the power deposition pattern required to maintain the target temperature distribution. Then the computed power distribution pattern can be approximated with a real applicator and scan path. The calculation of the desired power deposition pattern should also provide insight into the design of more useful applicators and scan paths. A technique for calculating power deposition patterns from temperature distributions follows.

2. Theory

The one-to-one nature of the relationship between a power deposition pattern and its associated temperature distribution makes possible the calculation of temperature distributions from power deposition patterns and vice versa. One direction of this one-to-one relationship is well known and easily observed, i.e. that under steady-state conditions, for a given region and boundary conditions, a given power distribution produces a single temperature distribution, in accordance with the steady-state bioheat transfer equation (eqn (1)). The one-to-one nature of this transformation in the other direction is demonstrated by the substitution of a given temperature distribution into the steady-state bioheat transfer equation (eqn (1)) to yield a single power distribution. Since a power distribution produces a single temperature distribution and a temperature distribution is associated with just one power distribution, the one-to-one relationship is established.

Practical limitations require that $Q_p \geq 0$ which, upon substitution into eqn (1), yields

$$\frac{W_b C_b T}{K} \geq \nabla^2 T. \tag{2}$$

The largest spatial rate of temperature change which satisfies this constraint is obtained by setting the two terms of eqn (2) equal, which is equivalent to setting $Q_p = 0$. Thus, by setting $Q_p = 0$ outside the tumour, the power deposition will be positive everywhere, and the rate of decrease of temperature with distance from the tumour boundary will be as large as possible. This approach has been used in all analyses which follow including the half-space, cylindrical and spherical tumour models illustrated in this section.

2.1. *Half-space tumour model*

To illustrate the calculation of the power deposition distribution from the temperature distribution, an analytical example is considered which consists of infinite half spaces of normal and tumour tissue. Since T will be a function of x only, the bioheat equation is reduced to its one-dimensional form and eqn (1) can be rewritten as

$$\frac{d^2T}{dx^2} - \frac{W_b C_b T}{K} + \frac{Q_p}{K} = 0. \tag{3}$$

The objective of this analysis is to determine the power deposition pattern required to maintain the temperature T of all points within the tumour, $x < 0$, at T_o and to elevate

the temperature of the normal tissue as little as possible.

For $x < 0$, the temperature is fixed at T_o and d^2T/dx^2 in this region is zero. Thus, in the tumour region, eqn (3) reduces to

$$Q_p = W_{bt} C_b T_o, \tag{4}$$

where the additional subscript t indicates values for tumour tissue. The value for W_{bt} can vary within the tumour region; but as long as $T = T_o$, eqn (4) holds and Q_p can be determined analytically.

In the region $x > 0$, eqn (3) takes the form

$$\frac{d^2T}{dx^2} - \frac{W_{bn} C_b T}{K_n} = 0 \tag{5}$$

since the area of consideration is outside the tumour region and no heat deposition in normal tissue is desired. The additional subscript n indicates values for normal tissue. Taking K_n, W_b and C_b to be constants; solving eqn (5) for T; and applying the boundary condition that $T = T_o$ at $x = 0$ gives

$$T = T_o \exp[-(W_{bn} C_b / K_n)^{\frac{1}{2}} x] \tag{6}$$

for the temperature in the normal tissue. A cross-section of the temperature T in the half-space model is shown in figure 1 (*a*).

Knowledge of the complete temperature distribution allows calculation of the power deposition pattern. The power deposition within the tumour region is given by eqn (4), and since power deposition in normal tissue was defined to be zero, the only remaining

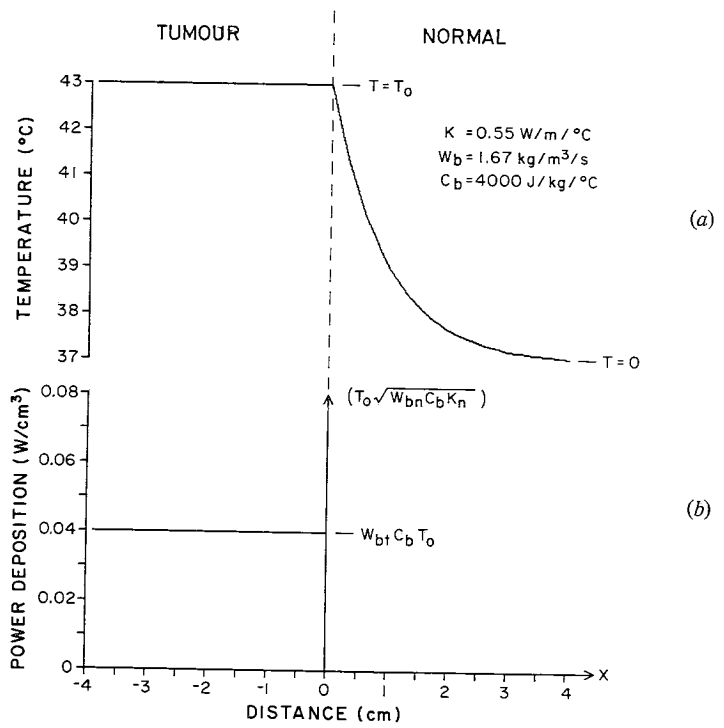

Figure 1. Temperature (*a*) and power deposition (*b*) distributions in the half-space tumour model.

power deposition to be determined is that at the tumour-normal tissue boundary. For the power deposition at the infinitely thin boundary to contribute to heating, it must be in the form of a delta function. Letting P be the strength of the delta function at the boundary, the power deposition is given by

$$Q_p = P\delta(x) + W_{bt}C_bT_ou(-x) \tag{7}$$

where $\delta(x)$ is a unit delta function centered on the tumour-normal tissue boundary and $u(-x)$ is a unit step function (1 for $x<0$, 0 for $x>0$). Substituting Q_p into eqn (3) and integrating from $x=0^-$ to 0^+ yields

$$P = -K\frac{dT(x)}{dx}\Bigg|_{0^-}^{0^+}. \tag{8}$$

Evaluating the derivative of T at $x=0^-$ and 0^+ and substituting into eqn (8) gives

$$P = T_o(W_{bn}C_bK_n)^{\frac{1}{2}}. \tag{9}$$

The complete power deposition pattern required to produce a uniform temperature within the tumour half space for this model is shown in figure 1 (*b*).

2.2. *Infinite cylinder tumour model*

A model also considered in this study is an infinitely long cylindrical tumour, which has application in many of the circularly symmetric bioheat transfer models. The infinite extent of the tumour limits the applicability of this model to approximations for the mid-section of a cylindrical tumour, although a complete analytical solution for a finite length cylindrical tumour could be solved using the same method. The bioheat transfer equation is transformed into cylindrical coordinates, with the angular and z-dependent terms omitted due to angular symmetry and infinite z extent, to yield

$$\frac{r^2d^2T}{dr^2} + \frac{rdT}{dr} - \frac{W_bC_br^2T}{K} + \frac{r^2Q_p}{K} = 0. \tag{10}$$

In the tumour region, where $r<r_o$, the temperature is fixed at T_o so that the derivatives of T are zero and eqn (10) reduces to eqn (4). In normal tissue, where $r>r_o$, the power deposition is taken as zero, and eqn (10) becomes

$$\frac{r^2d^2T}{dr^2} + \frac{rdT}{dr} - \frac{W_{bn}C_br^2T}{K_n} = 0. \tag{11}$$

Eqn (11) is Bessel's equation of order zero which has a solution of the form

$$T = GI_0((W_{bn}C_b/K_n)^{\frac{1}{2}}r) + HK_0((W_{bn}C_b/K_n)^{\frac{1}{2}}r) \tag{12}$$

where I_0 and K_0 are Bessel functions of imaginary arguments and G and H are constants. As r approaches infinity T must approach zero, but I_0 increases without bound, therefore the constant G must be zero. The constant H can be determined by evaluating eqn (12) (with $G=0$) at the boundary $r=r_o$, where $T=T_o$. Substitution of these constants into eqn (12) gives

$$T = \frac{T_oK_0(r(W_{bn}C_b/K_n)^{\frac{1}{2}})}{K_0(r_o(W_{bn}C_b/K_n)^{\frac{1}{2}})} \tag{13}$$

for $r \geq r_o$. The temperature distribution for this model is shown in figure 2 (*a*) as a function of radial distance.

The assumption of a delta function for the power deposition at the tumour-normal tissue boundary in the radial direction is made, analogous to that assumed for the half-

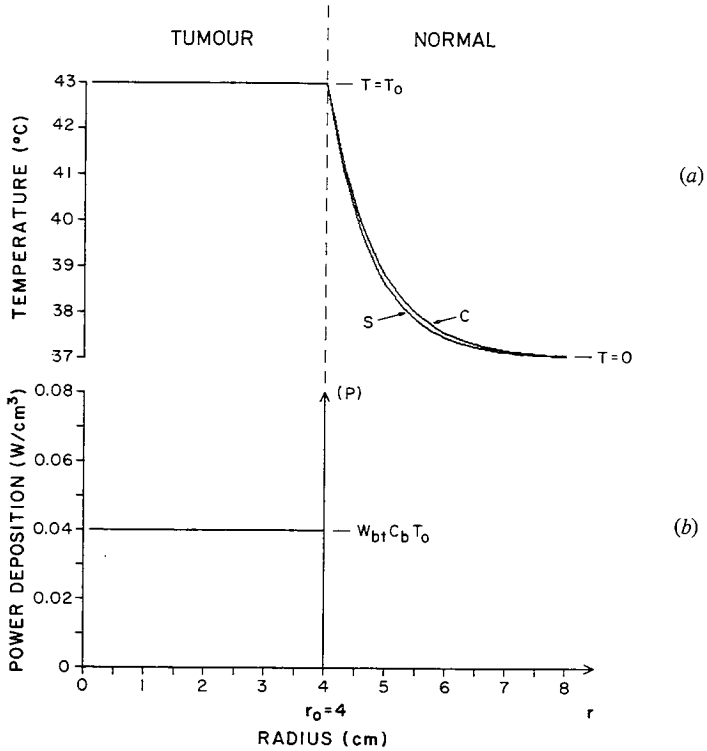

Figure 2. Temperature (*a*) and power deposition (*b*) distributions in the cylindrical (C) and spherical (S) tumour models. P is given by eqn (14) and eqn (19) for the cylinder and sphere, respectively.

space tumour model. Again, the strength of the delta function is taken as P and is found to be the difference of the derivatives of the temperature on each side of the tumour-normal tissue boundary times the thermal conductivity, which is evaluated to yield

$$P = T_o(W_{bn}C_bK_n)^{\frac{1}{2}} \frac{K_1(r_o(W_{bn}C_b/K_n)^{\frac{1}{2}})}{K_0(r_o(W_{bn}C_b/K_n)^{\frac{1}{2}})} \tag{14}$$

where K_0 and K_1 represent the zeroth and first-order K Bessel functions, respectively. The strength of the delta function at the boundary is dependent upon r_o, the radius of the tumour. The complete power deposition pattern for the cylindrical geometry is shown in figure 2 (*b*) as a function of radial distance.

2.3. *Spherical tumour model*

A more realistic analytical example is a spherical tumour surrounded by an infinitely extended region of homogeneous normal tissue. Though the normal tissue is infinite in extent, the model is applicable to most tumours because heat conduction in the normal tissue is limited to less than several centimeters when blood perfusion is considered. Equation (1) may be expressed in spherical coordinates with the angular dependent terms omitted, since no angular variation in temperature is desired, to yield

$$\frac{d^2T}{dr^2} + \frac{2dT}{rdr} - \frac{W_bC_bT}{K} + \frac{Q_p}{K} = 0. \tag{15}$$

For the tumour region, $r < r_o$, the temperature is fixed at T_o and the derivatives of T in this region are zero. As in the previous models, the bioheat equation in the tumour

region reduces to eqn (4). As noted previously, W_{bt} is not required to be constant with respect to r (in fact it can also vary with angular position) for this result to hold.

In the normal region, $r > r_o$, Q_p is zero and eqn (15) becomes

$$\frac{d^2T}{dr^2} + \frac{2dT}{rdr} - \frac{W_{bn}C_bT}{K_n} = 0 \tag{16}$$

which yields

$$T = \frac{A}{r}\exp[-(W_{bn}C_b/K_n)^{\frac{1}{2}}r] + \frac{B}{r}\exp[(W_{bn}C_b/K_n)^{\frac{1}{2}}r]. \tag{17}$$

Since T approaches zero as r approaches infinity, $B = 0$. Applying the boundary condition at r_o, i.e. $T = T_o$, the constant A is evaluated to give

$$T = \frac{T_o r_o}{r}\exp[(W_{bn}C_b/K_n)^{\frac{1}{2}}(r_o - r)] \tag{18}$$

for $r \geq r_o$. The complete temperature distribution is shown in figure 2 (*a*) as a function of the radial distance r.

The power deposition required at $r = r_o$ can now be calculated from the temperature distribution, and as before it is a delta function. The strength of the delta function P is again found to be the product of the thermal conductivity and the difference of the derivatives of the temperature on each side of the tumour-normal tissue boundary, and is evaluated to yield

$$P = T_o((W_{bn}C_bK_n)^{\frac{1}{2}} + K_n/r_o). \tag{19}$$

The complete power deposition pattern is shown in figure 2 (*b*).

2.4. *Properties of models*

The strength of the delta function at the tumour boundary is a constant for the half-space tumour model, a quotient of Bessel functions dependent upon tumour radius for the cylindrical tumour model, and a simple function of tumour radius for the spherical tumour model. The strength of the delta function is shown as a function of tumour radius in figure 3 for the three tumour models discussed. For larger tumour diameters, the strength approaches a constant value for all models, which could be used as an approximation for large tumours.

For the previous illustrations, W_b and K were chosen as constants to illustrate the analytical solution. Although these must be constant in the normal tissue they need not be constant within the tumour. Studies of tumour perfusion have shown that blood flow varies from near zero in the necrotic core to elevated values in the advancing front of the tumour (Endrich *et al.* 1979). An example of this situation is illustrated in figure 4.

3. Methods

Practically, tumours are not exactly spherical and tissue parameters are not constant, so the analytical solution presented in the previous section would seldom be applicable. A three-dimensional numerical solution to the problem has been developed using a finite difference solution (Myers 1971) to account for the various geometries and parameter variations encountered in a clinical situation.

The temperature distribution required for the numerical solution was determined by first setting the temperature in the tumour region to a constant value T_o and then calculating T outside the tumour using a finite difference solution to the steady-state bioheat

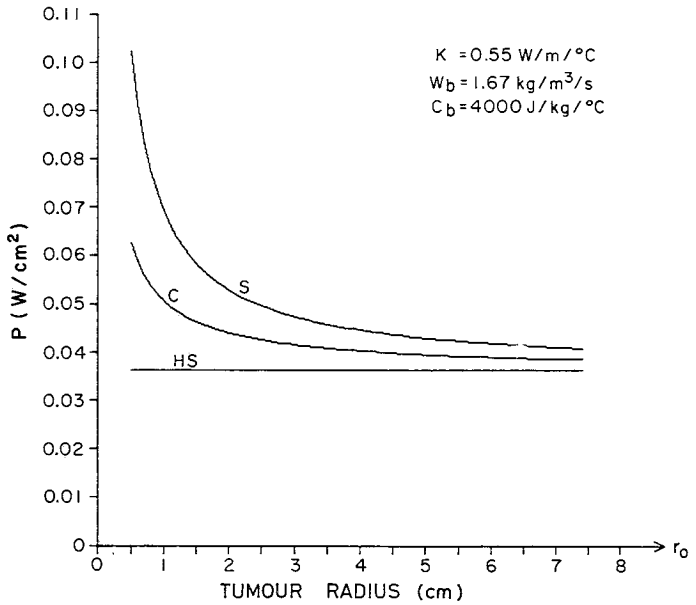

Figure 3. Strength of the delta function required at the tumour boundary versus tumour radius for the cylindrical (C) and spherical (S) models. The strength of the delta function required for the half-space model (HS) is included for comparison.

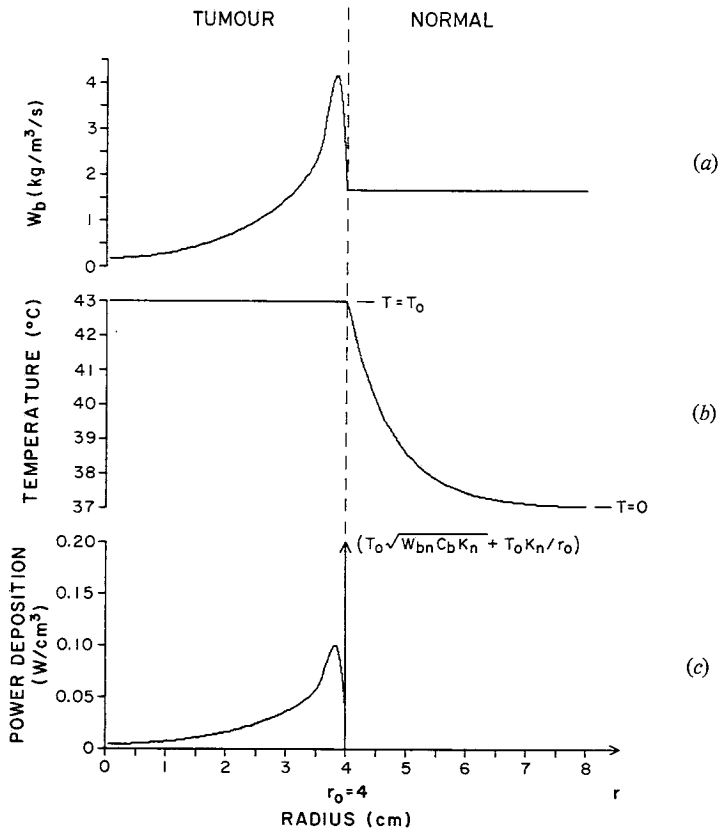

Figure 4. Example of variable perfusion within the tumour (*a*) and associated temperature (*b*) and power deposition (*c*) distributions for the spherical model.

transfer equation with $Q_p = 0$. Such a method ensures that the bioheat transfer equation is satisfied, only positive power deposition is required, and all tumour temperatures are held at a constant value T_o. The three-dimensional finite difference representation of the bioheat transfer equation used in this solution is given by

$$T_{k,m,n} = (K/(6K + d^2 W_b C_b))\,((d^2 Q_p/K) + T_{k-1,m,n} + T_{k+1,m,n} + T_{k,m-1,n} + T_{k,m+1,n} + T_{k,m,n-1} + T_{k,m,n+1}) \quad (20)$$

where k, m and n are the indices of the point at which the temperature is being calculated and d is the distance between sample points. The associated power deposition pattern is calculated from the temperature distribution by inverting eqn (20) to yield

$$Q_p = (K/d^2)(6T_{k,m,n} - T_{k-1,m,n} - T_{k+1,m,n} - T_{k,m-1,n} - T_{k,m+1,n} - T_{k,m,n-1} - T_{k,m,n+1}) + W_b C_b T_{k,m,n}. \quad (21)$$

The application of this equation to theoretical temperature distributions produces an accurate result as confirmed by comparison to the analytic examples illustrated in the Theory section.

4. Results

The three-dimensional numerical solution was applied to two tumour geometries. The first geometry was a 4 cm cubic tumour centred at 6 cm from the skin surface. For this particular example, tumour and skin temperatures of 43 and 25°C, respectively, were chosen. Cross-sections of the complete temperature profile and associated power deposition pattern, through the centre of the tumour, are shown in figure 5. The power deposition pattern exhibits the large maxima near the tumour boundary analogous to those seen in the analytic models. The constant value evident in the central region of the tumour is a result of the use of a constant value for W_{bt} in this example.

The second tumour geometry consisted of a 4 cm diameter spherical tumour located 6 cm from the body surface. Figure 6 shows cross-sections of the temperature profile and associated power deposition pattern through the centre of the tumour. The high power deposition on the periphery of the tumour in figure 6 represents the delta function in the theoretical models, and the variation in the power deposition at the periphery is due to the imperfect representation of the spherical boundary in a rectangular co-ordinate system. This results in variations in the local curvature of the tumour boundary and the effective radius of the tumour, yielding a varying power deposition on the tumour periphery in accordance with eqn (19).

5. Discussion

Currently, most investigators select a hyperthermia system and then select placement of sources, initial field configuration, or an initial scan path based on experience and intuition. For the choice of initial field configuration and scan path, modifications are made in an iterative manner based on calculations using the bioheat transfer equation prior to treatment, or during treatment based on temperature feedback. The ultimate goal of this study is to determine an approach which will allow direct calculation of the initial treatment configuration based on the desired temperature profile, tissue thermal properties including blood perfusion, and hyperthermia system parameters such as beam size for a scanned ultrasound applicator.

As a first step towards this goal, a three-dimensional numerical method for calculating the optimum power deposition pattern given the desired tumour temperature was presented in this paper. The method can be applied to the complex tumour geometries

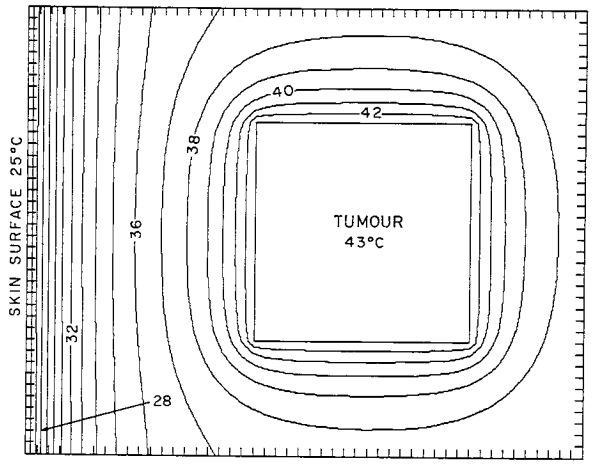

(*a*)

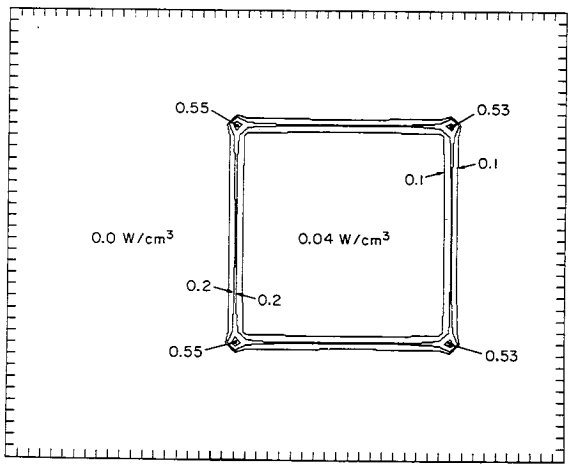

(*b*)

Figure 5. Contour plots of a cross-section of the temperature (*a*) and power deposition (*b*) distributions for a numerically calculated cubical tumour model sampled every 2 mm. Temperature contours are shown for 1°C increments and power deposition contours are given for 0·1 W/cm^3, 0·2 W/cm^3, and 0·4 W/cm^3.

which are encountered clinically and to tumours with non-uniform temperature-dependent perfusion. The other stages of this study deal with examination of the initial heating of the tumour and with techniques for generating the treatment configuration which will most nearly produce the desired power deposition pattern. The analysis considers the effect of such parameters as the heating profile around implantable sources, multiple focus systems, and the beam size and scan path. The results of these analyses are treated in a separate paper.

Acknowledgments

This study was supported in part by Labthermics Technologies, Inc., and in part by a fellowship from the Caterpillar Corporation. The authors are thankful to C. A. Cain, R. L. Magin and J. F. McCarthy for helpful discussions.

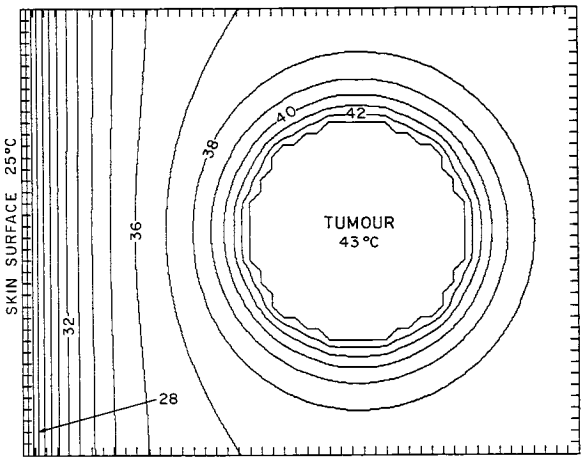

(*a*)

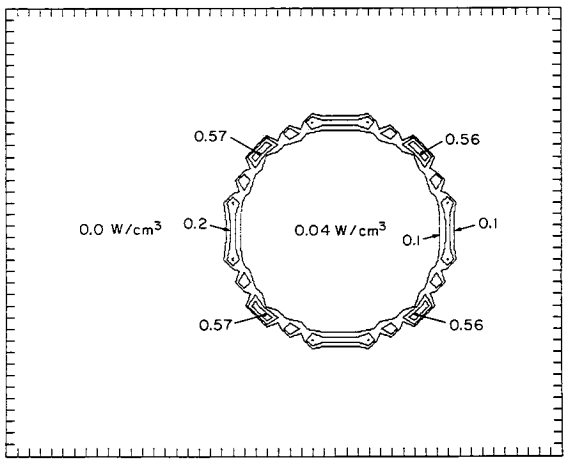

(*b*)

Figure 6. Contour plots of a cross-section of the temperature (*a*) and power deposition (*b*) distributions for a numerically calculated spherical tumour model sampled every 2 mm. Temperature contours are shown for 1°C increments and power deposition contours are given for 0·1 W/cm^3, 0·2 W/cm^3, and 0·4 W/cm^3.

References

BOWMAN, H. F., 1981, Heat transfer and thermal dosimetry. *Journal of Microwave Power*, **16,** 121–133.

CHEN, M. M., and HOLMES, K. R., 1980, Microvascular contributions in tissue heat transfer. *Annals of New York Academy of Sciences*, **335,** 137–150.

CHRISTENSEN, D. A., and DURNEY, C. H., 1981, Hyperthermia production for cancer therapy: a review of fundamentals and methods. *Journal of Microwave Power*, **16,** 89–105.

CRAVALHO, E. G., FOX, L. R., and KAN, J. C., 1980, The application of the bioheat equation to the design of thermal protocols for local hyperthermia. *Annals of the New York Academy of Sciences*, **335,** 86–97.

DICKINSON, R. J., 1984, An ultrasonic system for local hyperthermia using scanned focused transducers. *IEEE Transactions Biomedical Engineering*, **31,** 120–125.

ENDRICH, B., REINHOLD, H. S., GROSS, J. F., and INTAGLIETTA, M., 1979, Tissue perfusion inhomogeneity during early tumor growth in rats. *Journal of the National Cancer Institute*, **62,** 387–393.

HYNYNEN, K., 1986, Generation of ultrasonic fields and the acoustic properties of tissues. *Hyperthermia*, edited by D. J. Watmough and W. M. Ross (Glasgow: Blackie & Son Limited), pp. 76–98.

JAIN, R. K., 1983, Bioheat transfer: mathematical models of thermal systems. *Hypertherma in Cancer Therapy*, edited by F. K. Storm (Boston: Hall Medical Publishers), pp. 9–46.

KANTOR, G., 1981, Evaluation and survey of microwave and radiofrequency applicators. *Journal of Microwave Power*, **16,** 135–150.

MYERS, G. E., 1971, *Analytical Methods in Conduction Heat Transfer* (New York: McGraw-Hill), pp. 233–319.

OLESON, J. R., 1984, A review of magnetic induction methods for hyperthermia treatment of cancer. *IEEE Transactions Biomedical Engineering*, **31,** 91–97.

ROEMER, R. B., SWINDELL, W., CLEGG, S. T., and KRESS, R. L., 1984, Simulation of focused, scanned ultrasonic heating of deep-seated tumors: the effect of blood perfusion. *IEEE Transactions Sonics and Ultrasonics*, **31,** 457–466.

STAUFFER, P. R., CETAS, T. C., FLETCHER, A. M., DEYOUNG, D. W., DEWHIRST, M. W., OLESON, J. R., and ROEMER, R. B., 1984, Observations on the use of ferromagnetic implants for inducing hyperthermia. *IEEE Transactions Biomedical Engineering*, **31,** 76–90.

STORM, F. K., MORTON, D. L., KAISER, L. R., HARRISON, W. H., ELLIOTT, R. S., WEISENBURGER, T. H., PARKER. R. G., and HASKELL, C. M., 1980, Clinical radio-frequency hyperthermia: a review. *National Cancer Institute Monographs*, **61,** 343–350.

STROHBEHN, J. W., and ROEMER, R. B., 1984, A survey of computer simulations of hyper-thermia treatments. *IEEE Transactions Biomedical Engineering*, **31,** 136–149.

TAYLOR, L. S., 1980, Implantable radiators for cancer therapy by microwave hyperthermia. *Proceedings of the IEEE*, **68,** 142–149.